SiGeC Near Infrared Photodetectors

Baojun Li[1], Soo-Jin Chua[1,2,4], E. A. Fitzgerald[1,3], C. W. Leitz[1,3], and Lingyun Miao[1,4]

[1]*Advance Materials for Micro- and Nano- Systems Programme, Singapore-MIT Alliance, Singapore 119260, Singapore*
[2]*Department of Electrical and Computer Engineering, National University of Singapore, Singapore 117576, Singapore*
[3]*Department of Materials Science and Engineering, Massachusetts Institute of Technology, Cambridge, Massachusetts 02139, USA*
[4]*Institute of Materials Research and Engineering, Singapore 117602, Singapore*

***Abstract*–A near infrared waveguide photodetector in Si-based ternary $Si_{1-x-y}Ge_xC_y$ alloy was demonstrated for 0.85~1.06 μm wavelength fiber-optic interconnection system applications. Two sets of detectors with active absorption layer compositions of $Si_{0.79}Ge_{0.2}C_{0.01}$ and $Si_{0.70}Ge_{0.28}C_{0.02}$ were designed. The active absorption layer has a thickness of 120~450 nm. The external quantum efficiency can reach ~3% with a cut-off wavelength of around 1.2 μm.**

***Index Terms*–Photodetector, quantum efficiency, absorption coefficient, absorption efficiency, band gap, lattice constant, critical thickness, SiGeC, semiconductor, alloy.**

I. INTRODUCTION

Epitaxial layers based on group IV elements and grown on Si substrate extend the use of material composition in new device concepts for silicon microelectronic technology. In the group IV systems, SiGe grown on Si(100) is the most investigated heteroepitaxial layers. Si-based band gap engineering has made possible applications for epitaxial SiGe alloys in higher speed devices and also new optoelectronic devices. Such devices are the heterojunction bipolar transistor, metal-oxide-semiconductor field effect transistor, photodiode and photodetector. Among these devices, photodetectors based on SiGe and SiGe/Si multiple-quantum well (MQW) have been extensively studied [1]–[15] and most were fabricated as waveguide configurations due to the small absorption coefficient for its indirect band gap. However, the SiGe system grown on Si(100) substrate exhibits some severe limitations, such as the existence of a critical thickness for perfect strain layer growth that depends on the amount of germanium. Above the critical thickness strain-relief occurs by injection and propagation of misfit dislocations. In addition, metastable SiGe layers (thicker than the critical thickness and grown at low temperature) tend to relax during post-growth thermal treatments, typical for device processing. Therefore, the thickness has to be kept always below the critical thickness. On the other hand, the high compressive strain present in the SiGe active layers imposes limits on the Ge fraction, the layer thickness as well as on the temperature of processing steps subsequent to the SiGe layer deposition. The fundamental limitation of SiGe alloys on Si substrate for detector applications is the large lattice mismatch between SiGe and Si, especially for SiGe with a high Ge fraction. In order to obtain sufficient absorption at near-infrared wavelengths, the Ge content should be greater than 50%. For 60% Ge content the critical thickness is less than 10 nm. This thickness is too small for efficient optical detection. By using MQW structure with $Si_{0.5}Ge_{0.5}$ layer sandwiched between Si layers

in a thickness ratio of one to five, the overall thickness of the SiGe is still limited to about 100 nm. Although the use of a graded buffer structure may solve the lattice mismatch problem, the large buffer layer thickness (typically 1 μm for every 10% Ge) requires a much longer growth time.

In order to reduce the strain in SiGe alloys and eliminate the aforementioned problems so that one can achieve high efficiency detector near infrared wavelength without resorting to sophisticated processing or growth procedure, a possible approach is to go beyond the SiGe binary alloy system. Ternary $Si_{1-x-y}Ge_xC_y$ alloy is a possible candidate. The lattice constant of carbon in the diamond structure is 0.3545 nm smaller than that of Si (0.5431 nm) and Ge (0.5646 nm). Only small amounts of carbon are needed for significant strain compensation. A 1% substitutional carbon content would compensate the strain in a ~10% SiGe alloy, thus relaxing the Ge fraction and the SiGe thickness constraints imposed by higher temperature processing steps on SiGe layers. The advantages of $Si_{1-x-y}Ge_xC_y$/Si for optoelectronic devices are the adjustable strain, band gap, and band offsets. According to the Vegard's law, the lattice-matched composition of $Si_{1-x-y}Ge_xC_y$ alloys to Si is $Si_{1-9.2y}Ge_{8.2y}C_y$ [16]. At present, the $Si_{1-x-y}Ge_xC_y$ optical waveguide [17] and photodetectors [18], [19] have already been reported. In the literatures [18] and [19], the compositions are 55~60%Ge with 1.5%C and the peak response wavelength is around 0.85-0.95 μm. Due to the wavelengths range from 0.85–1.06 μm are the fiber-optic interconnection wavelengths used in low-cost, reliable, high-performance silicon-based optoelectronic integrated circuits (OEICs) and at present, no $Si_{1-x-y}Ge_xC_y$ alloys detector was reported in this wavelength range. In this work, two sets of low Ge and C composition detectors were designed and demonstrated. The cut-off wavelength of the detector is around 1.2 μm. The structure with lower Ge and C compositions in $Si_{1-x-y}Ge_xC_y$ active absorption layers are very easy to grow at 500~600 °C by molecular beam epitaxy (MBE) or rapid thermal chemical vapor deposition (RTCVD).

II. DETECTION CONFIGURATION

Fig. 1 shows the schematic diagram of a $Si_{1-x-y}Ge_xC_y$ alloy photodetector. The detector is a waveguide configuration and consists of an unintentionally doped $Si_{1-x-y}Ge_xC_y$ active absorption layer, a heavily doped Si top cap layer, and two lightly doped Si buffer layers. The two lightly doped buffer layers are placed on top and bottom of $Si_{1-x-y}Ge_xC_y$ active layer, respectively. Devices can be shaped by conventional photolithography and dry or wet chemical etching. The thickness of the cap layer is ~20 nm and of the buffer layer is ~100 nm. The thickness of $Si_{1-x-y}Ge_xC_y$ active absorption layer has been designed to enable light beam coupled into the active absorption layer from a side facet. The width is around 10 μm which matched the core diameter of single-mode fiber.

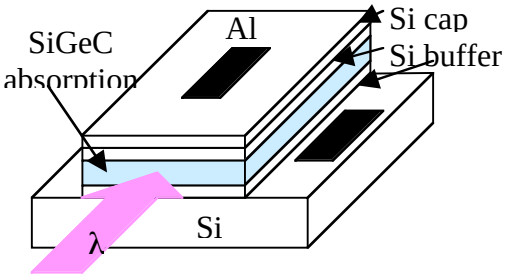

Fig. 1. Schematic diagram of a $Si_{1-x-y}Ge_xC_y$ alloy photodetector considered for demonstration.

III. THEORETICAL ANALYSIS

3.1 Lattice constant and misfit

Carbon with a lattice parameter of 0.3545 nm is much smaller than the lattice size of Si (0.5431 nm) and Ge (0.5646 nm). The lattice mismatch between Si and diamond is 52% compared to only 4% between Si and Ge. In other words, a strained diamond film on Si would have to be laterally extended by 52% to match the Si substrate. This means that only a very small amount of substitutional C in Si is necessary to introduce large average tensile strain in the strained epilayer. Assuming a linear dependence of the intrinsic lattice constant $a_0(x, y)$ of $Si_{1-x-y}Ge_xC_y$ on the composition x and y between Si, Ge, and

diamond one gets the following expression [20]:

$$a_0(x, y) = a_{Si} + x(a_{Ge} - a_{Si}) + y(a_C - a_{Si}) \quad (1)$$

where a_{Si}, a_{Ge}, and a_C are the lattice constants of silicon, germanium, and diamond, respectively. Based on this linear interpolation it turns out that the compressive strain of 8.2% Ge can be compensated by 1% C in strained $Si_{1-x-y}Ge_xC_y$ layer on Si substrate. By using a linear interpolation between SiC, Si and Ge, the lattice constant of $Si_{1-x-y}Ge_xC_y$ can be expressed as:

$$a_0(x, y) = a_{Si} + x(a_{Ge} - a_{Si}) + 2y(a_{SiC} - a_{Si}) \quad \text{for } 0 < y < 0.5 \quad (2)$$

This formula provides strain compensation for 9.4% Ge by 1% C. The difference is due to the fact that a_{SiC} is not exactly in the middle between a_{Si} and a_C. Moreover, a_{SiC} is 0.436 nm, whereas $(a_{Si} + a_C)/2$ is 0.461 nm.

Assuming that Vegard's law is valid, the misfit parameter for the $Si_{1-x-y}Ge_xC_y$ layers grown on Si substrate can be written as:

$$f_m = (a_{SiGeC} - a_{Si})/a_{Si} = [x(a_{Ge} - a_{Si}) + y(a_C - a_{Si})]/a_{Si} \quad (3)$$

From Eq. (3) we can see that carefully chosen composition x and y can decrease the mismatch dislocation between $Si_{1-x-y}Ge_xC_y$ layer and the Si substrate.

3.2 Absorption coefficient

Since the quantum efficiency of the detector strongly depends on the materials absorption coefficient, an estimate of the absorption coefficient as a function of photon energy and Ge and C compositions of the alloy is necessary. $Si_{1-x-y}Ge_xC_y$ indirect absorption process depends on the interaction of electron and electromagnetic wave and at the same time, depends on the interaction of electron and lattice. The fundamental absorption coefficient α can be expressed as [21]:

$$\alpha = A_a \frac{(h\nu - E_g + E_p)^2}{\exp(E_p / kT) - 1} + A_e \frac{(h\nu - E_g - E_p)^2}{1 - \exp(-E_p / kT)} \quad h\nu > E_g + E_p \quad (4)$$

$$\alpha = A_a \frac{(h\nu - E_g + E_p)^2}{\exp(E_p / kT) - 1} \quad E_g - E_p < h\nu \le E_g + E_p \quad (5)$$

$$\alpha = 0 \quad h\nu \le E_g - E_p \quad (6)$$

where $h\nu$ is the photon energy, E_g is the indirect bandgap of $Si_{1-x-y}Ge_xC_y$ alloy, E_p is the phonon energy, T is the temperature, k is Boltzmann constant, and the parameters A_a and A_e weigh the phonon absorption and emission contributions, respectively.

3.3 Absorption efficiency and external quantum efficiency

For waveguide configuration detector, the absorption efficiency η_{eff} of $Si_{1-x-y}Ge_xC_y$ layer as a function of the layer thickness (d) and optical absorption coefficient (α) satisfies [11]:

$$\eta_{eff} = 1 - \exp(-\alpha d) \quad (7)$$

The external quantum efficiency η_{ext} can be expressed as [6]:

$$\eta_{ext} = C(1 - R)(1 - e^{-\alpha \Gamma f L}) \quad (8)$$

where C is the coupling efficiency of fiber-to-waveguide detector. R is the power reflectivity of air-semiconductor interface, α is the absorption coefficient of $Si_{1-x-y}Ge_xC_y$ alloy, f is a ratio expressing the volume of $Si_{1-x-y}Ge_xC_y$ alloy layer with respect to the total volume of the detection layers, L is the detection length, and Γ is the optical power confinement factor within the $Si_{1-x-y}Ge_xC_y$ detection layer and can be described as:

$$\Gamma = \frac{\iint_{active-absorption-layer} |E(x,y)|^2 \, dx \, dy}{\iint_{\infty} |E(x,y)|^2 \, dx \, dy} = \frac{\int_{x-active-layer} |E_x(x)|^2 \, dx}{\int_{-\infty}^{\infty} |E_x(x)|^2 \, dx} \cdot \frac{\int_{y-active-layer} |E_y(y)|^2 \, dy}{\int_{-\infty}^{\infty} |E_y(y)|^2 \, dy} = \Gamma_x \Gamma_y \quad (9)$$

where $E(x, y)$ is the transverse electric field profile in the $Si_{1-x-y}Ge_xC_y$ detection layer.

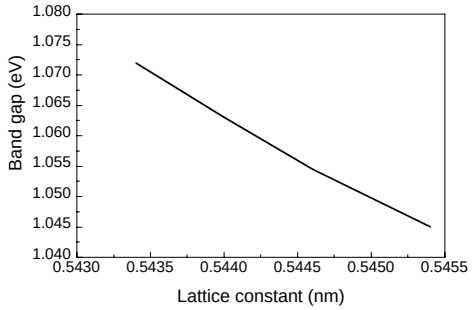

Fig. 2. Band gap versus lattice constant for a strained $Si_{1-x-y}Ge_xC_y$ alloy.

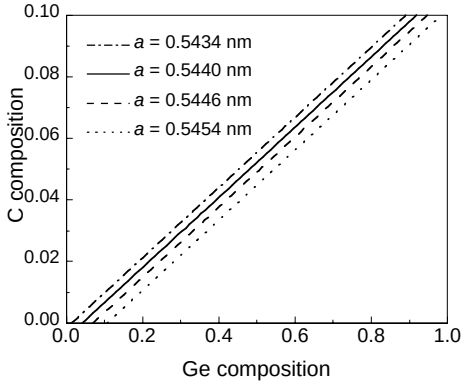

Fig. 3. C and Ge compositions in $Si_{1-x-y}Ge_xC_y$ alloy at different lattice constants.

IV. CALCULATION AND DISCUSSION

4.1 Band gap, lattice constant and composition

Experimental indirect band gaps are 5.5 eV for C, 1.13 eV for Si, and 0.67 eV for Ge. Soref had estimated the band gap of ternary semiconductor $Si_{1-x-y}Ge_xC_y$ versus lattice parameter and composition [22] and shown that the absorption edges of the materials cover the near-infrared, visible, and near-ultraviolet ranges. Fig. 2 shows the band gap of a strained $Si_{1-x-y}Ge_xC_y$ alloy versus lattice constant came from the literature [23]. From Fig. 2 we can see that for the strained $Si_{1-x-y}Ge_xC_y$ alloy, the lattice constant is between 0.5434~0.5454 nm and the band gap is about 1.045~1.073 eV. This means that if use strained $Si_{1-x-y}Ge_xC_y$ alloy as the active absorption layer in detectors, the maximum absorption wavelength can reach 1.16~1.19 μm and varied with composition of x and y. Fig. 3 shows the possible C and Ge compositions in $Si_{1-x-y}Ge_xC_y$ alloy for different lattice constants obtained according to Eq. (1). A high C concentration will lead to a crystallographic degradation of the layer [24]. Carbon concentrations above 5 at.% starts to destroy the epitaxial relation between the layer and the substrate and a long growth time is also needed. In order to maintain high quality and at the same time easy to grow, two low C compositions of $Si_{0.79}Ge_{0.2}C_{0.01}$ and $Si_{0.70}Ge_{0.28}C_{0.02}$ were considered for compressive strain materials. According to Eq. (3), the mismatches of $Si_{0.79}Ge_{0.2}C_{0.01}$ and $Si_{0.70}Ge_{0.28}C_{0.02}$ layer with Si substrate are 0.44% and 0.41%, respectively. This is matched very much with the 0.52% for $Si_{0.785}Ge_{0.205}C_{0.01}$ reported in Ref. [17].

4.2 Critical thickness

The MBE growth of strained $Si_{1-x-y}Ge_xC_y$ layers is a much complicated process than the growth of SiGe layers. There is only a narrow temperature window for good epitaxial growth using atomic sources. At lower substrate temperatures, i.e. below 400 °C, twinning leads to amorphous growth as the temperature is reduced or the carbon content of the layer increases. If the substrate temperature is above 600 °C the metastable regime does not exist and instead a mixed alloy carbide phase is produced. The carbide phase becomes dominant at higher temperatures. Thus in order to achieve high-quality expitxial materials, the $Si_{1-x-y}Ge_xC_y$ growth should be carried out in a temperature window between 400 and 600 °C [25]. For rapid thermal chemical vapor deposition (RTCVD), layers grown at 650 °C were of good quality as reported in [26] but if the growth temperatures are too high, some of the C atoms will be incorporated either as clusters or as SiC and will also decrease the critical thickness for strained layer growth. At lower temperatures, the growth will become very slow. From the viewpoint of growth, 500

550 and 600 °C were used in this work. According to the rule of 1% C compensating 8.2% Ge in strained $Si_{1-x-y}Ge_xC_y$ layer on Si substrate, the equivalent binary composition alloy of $Si_{0.882}Ge_{0.118}$ and $Si_{0.884}Ge_{0.116}$ with similar strain with ternary $Si_{0.79}Ge_{0.2}C_{0.01}$ and $Si_{0.70}Ge_{0.28}C_{0.02}$ alloy were obtained. Therefore, the critical thickness for both $Si_{0.882}Ge_{0.118}$ and $Si_{0.884}Ge_{0.116}$ layers and also for $Si_{0.79}Ge_{0.2}C_{0.01}$ and $Si_{0.70}Ge_{0.28}C_{0.02}$ layers are 500, 175, and 150 nm at the growth temperatures of 500, 550, and 600 °C, respectively [27].

4.3 Absorption coefficient and absorption efficiency

The values of parameters A_a and A_e in Eq. (4)~(6) were obtained by using the equivalent binary alloy of $Si_{0.882}Ge_{0.118}$ and $Si_{0.884}Ge_{0.116}$ and are A_a = 11000 and A_e = 3000 for both $Si_{0.79}Ge_{0.2}C_{0.01}$ and $Si_{0.70}Ge_{0.28}C_{0.02}$ alloy [6]. The band gap of $Si_{0.79}Ge_{0.2}C_{0.01}$ and $Si_{0.70}Ge_{0.28}C_{0.02}$ is E_g = 1.045 eV and $h\nu$ = 1.052 eV (~1.187 μm). Usually, the phonon energy E_p is less than several percent, e.g. 2.58×10^{-2} eV. So the absorption coefficient α satisfies Eq. (5) and the results were shown in Fig. 4. From Fig. 4 we can see that the absorption coefficient is very small when the wavelength is near 1.2 μm. This indicates that for $Si_{0.79}Ge_{0.2}C_{0.01}$ or $Si_{0.70}Ge_{0.28}C_{0.02}$ active absorption layer detector, the maximum absorption cut-off wavelength is limited to 1.2 μm. It should be mentioned that the cut-off wavelength could be adjusted by the choice of the Ge and C contents.

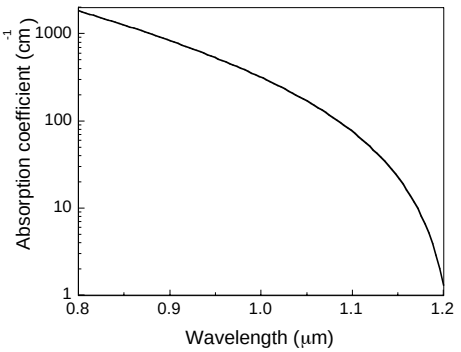

Fig. 4. Estimated absorption coefficient for strained $Si_{1-x-y}Ge_xC_y$ alloy versus absorption wavelengths.

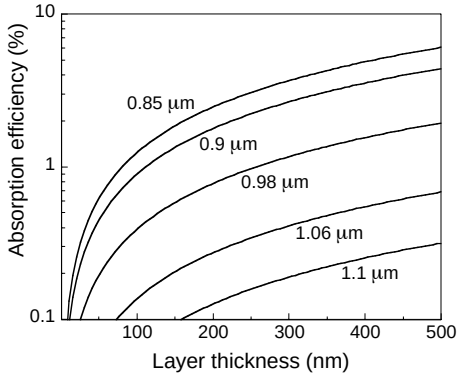

Fig. 5. The absorption efficiency versus the layer thickness at different wavelengths for strained $Si_{1-x-y}Ge_xC_y$ alloys.

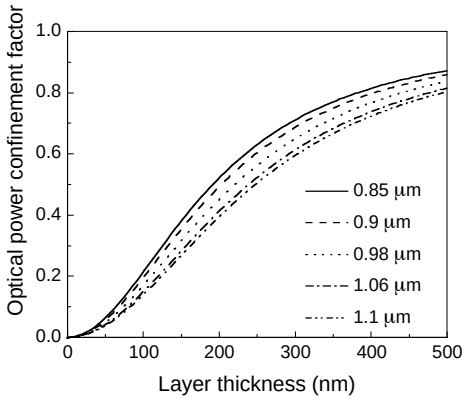

Fig. 6. The optical power confinement factor versus the $Si_{1-x-y}Ge_xC_y$ active absorption layer thickness at different wavelengths.

The absorption efficiency, η_{eff}, is a function of the layer thickness (d) and optical absorption coefficient (α). Fig. 5 shows the η_{eff} versus the layer thickness at different wavelength obtained according to Eq. (7). From Fig. 5 we can see that at less than the maximum critical thickness of 500 nm at 500 °C, the active absorption layers have a strong absorption efficiency in the optical interconnection wavelength of 0.85–1.06 μm.

4.4 External quantum efficiency

In order to estimate the external quantum efficiency, firstly, optical power confinement factor within the active absorption layer

should be obtained. By calculating Eq. (9) for the fundamental guided mode, the confinement factor Γ versus the active absorption layer thickness at different wavelengths was shown in Fig. 6. In the calculation, the refractive index of 3.5 for Si and 3.64 for SiGeC layer were used. Fig. 6 shows at the maximum critical layer thickness of 500 nm (for the growth temperature of 500 °C), the maximum confinement factor for 0.85~1.1 μm wavelength is around 80%. With the decrease of the detection layer thickness, the confinement factor along with the absorption efficiency will decrease. If the detection layer is too thin, the confinement factor and the absorption efficiency are also too small and will affect the external quantum efficiency of the detector. So below the layer critical thickness, the active absorption layer should be as thick as possible. By calculating Fresnel's equation for normal incidence, the reflectivity R of the air-semiconductor interface in Eq. (8) was about 56.9% for both $Si_{0.79}Ge_{0.2}C_{0.01}$ and $Si_{0.70}Ge_{0.28}C_{0.02}$ compositions detectors. The coupling efficiency C of the fiber-to-waveguide and the ratio f of the volume of $Si_{1-x-y}Ge_xC_y$ alloy layer with respect to the total volume of the detection layers were calculated and shown in Fig. 7. In the calculation, the coupling efficiency C was obtained according to the ratio of optical sensitive portion of the detector with the cross-section area of the fiber. The core diameter of single-mode fiber and the width of this waveguide detector were chosen to be 10 μm. Finally, the external quantum efficiencies (η_{ext}) were calculated. Figs. 8, 9 and 10 show the external quantum efficiency (η_{ext}) versus the detection length at different thickness of the active absorption layers for three typical wavelengths. From Fig. 8 we can see that for 0.85 μm wavelength, the detection external quantum efficiency can be higher than 1% and reach 3% at a very short detection length of 200 nm. For 0.9 μm wavelength (Fig. 9), at a short length of 300 nm, the detectors also have high external quantum efficiencies and are almost the same as of 0.85 μm wavelength. Even at the Si absorption edge of 1.1 μm (Fig. 10), the detectors also have strong absorptions. For example, at the detection length of 1 mm, the external

active absorption layer of 450 nm is 2.1%. The maximum external quantum efficiency can reach 3% at a little long detector length.

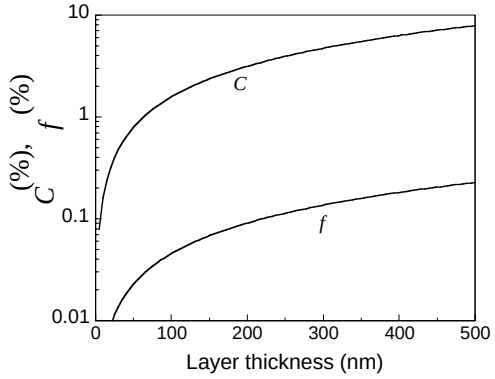

Fig. 7. The coupling efficiency C of the fiber-to-waveguide and the ratio f of the volume of $Si_{1-x-y}Ge_xC_y$ alloy layer with respect to the total volume of the detection layers versus the layer thickness.

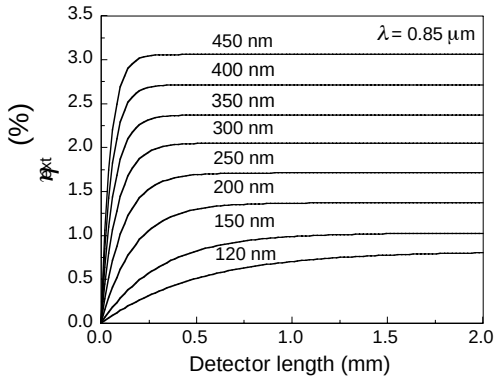

Fig. 8. External quantum efficiency (η_{ext}) as a function of detection length at different active absorption layers for the wavelength of 0.85 μm.

Fig. 11 shows the final layer structure and thickness of the photodecector obtained in this work with a cut-off wavelength of 1.2 μm The layers can be grown by MBE or RTCVD methods at 500, 550, and 600 °C. It should be emphasized that this waveguide detector has very low Ge and C compositions compared with the SiGeC detector reported in the literatures [18] and [19]. According to above calculation, by using a MQW structure with a strained alloy sandwiched layer between Si layers, the overall absorption layer thickness,

factor will increase and thus the quantum efficiency can be further enhanced.

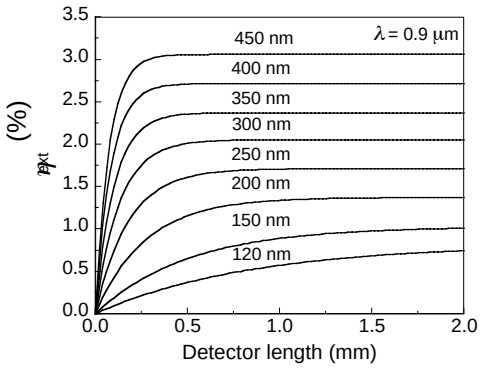

Fig. 9. External quantum efficiency (η_{ext}) as a function of detection length at different active absorption layers for the wavelength of 0.9 μm.

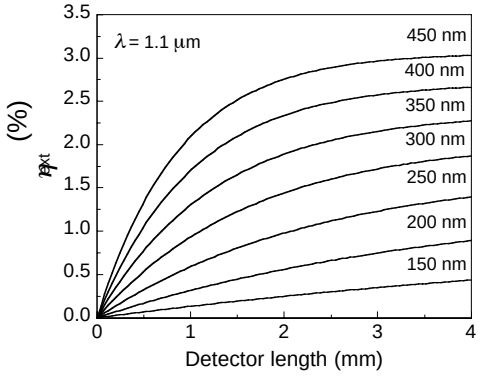

Fig. 10. External quantum efficiency (η_{ext}) as a function of detection length at different active absorption layers for the wavelength of 1.1 μm.

p^+-Si cap layer, 20 nm
p-Si buffer layer, 100 nm
i-$Si_{0.79}Ge_{0.2}C_{0.01}$ or i-$Si_{0.70}Ge_{0.28}C_{0.02}$ 120~450 nm (500 °C) or 120~150 nm (550 °C) or 120 nm (600 °C)
n-Si buffer layer, 100 nm
n^+-Si(100) Substrate

Fig. 11. The final waveguide photodetector layer structure and thickness for MBE or RTCVD growth at 500, 550, and 600 °C, respectively.

V. CONCLUSION

Two new compositions of $Si_{0.79}Ge_{0.2}C_{0.01}$ and $Si_{0.70}Ge_{0.28}C_{0.02}$ alloys near infrared waveguide photodetectors were proposed for fiber-optic communication system applications. The width of the waveguide detectors is 10 μm and the thickness of the active absorption layer is between 120~450 nm below the critical layer thickness. The detection active absorption layers have lower compositions of Ge (20~28%) and C (1~2%) and high absorption efficiency in the 0.85~1.06 μm wavelength range. The external quantum efficiency can be as high as 3.0% and the maximum absorption wavelength can reach 1.2 μm. These detector structures are very easy to grow at 500~600 °C by MBE or RTCVD methods and are very suitable for the monolithic integration with Si-based SiGe(C) optical waveguide devices. By using MQW structure with a strained SiGeC alloy sandwiched between Si layers, the overall absorption layer thickness, the coupling efficiency, and the confinement factor will increase and thus the quantum efficiency can be further enhanced.

REFERENCES

[1] H. Temkin, T. P. Pearsall, J. C. Bean, R. A. Logan, and S. Luryi,"Ge_xSi_{1-x} strained-layer superlattice waveguide photodetectors operating near 1.3 μm," *Appl. Phys. Lett.*, vol. 48(15), pp. 963–965, 1986.

[2] T. P. Rearsall, H. Temkin, J. C. Bean, and S. Luryi,"Avalanche gain in Ge_xSi_{1-x}/Si infrared waveguide detectors," *IEEE Electron Device Lett.*, vol. 7(5), pp. 330–332, 1986.

[3] T. L. Lin, J. S. Park, S. D. Gunapala, E. W. Jones, and H. M. Del Castillo,"Photoresponse model for $Si_{1-x}Ge_x$/Si heterojunction internal photoemission infrared detector," *I E E E Electron Device Lett.*, vol. 15(3), pp. 103–105, 1994.

[4] P. Kruck, M. Helm, T. Fromherz, G. Bauer, J. F. Nutzel, and G. Abstreiter, "Medium-wavelength, normal-incidence, p-type Si/SiGe quantum well infrared photodetector with background limited performance up to 85 K," *Appl. Phys. Lett.*, vol. 69(22), pp. 3372–3374, 1996.

[5] R. T. Carline, D. J. Robbins, M. B. Stanaway, and W. Y. Leong,"Long-wavelength SiGe/Si

resonant cavity infrared detector using a bonded silicon-on-oxide reflector," *Appl. Phys. Lett*., vol. 68(4), pp. 544–546, 1996.

[6] L. Naval, B. Jalali, L. Gomelsky, and J. M. Liu, "Optimization of $Si_{1-x}Ge_x$/Si waveguide photodetectors operation at λ = 1.3 μm," *J. Lightwave Technol*., vol. 14(5), pp. 787–797, 1996.

[7] C. Engel, P. Baumgartner, H. Holzmann, J. F. Nutzel, and G. Abstreiter, "Lateral photodector devices on Si/SiGe heterostructures," *Thin Solid Films*, vol. 294(1-2), pp. 347–350, 1997.

[8] H. Presting, "Near and mid infrared silicon/germanium based photodetection," *Thin Solid Films*, vol. 321, pp. 186–195, 1998.

[9] R. T. Carline, V. Nayar, D. J. Robbins, and M. B. Stanaway, "Resonant cavity longwave SiGe-Si photodetector using a buried silicide mirror," *IEEE Photon. Technol. Lett.*, vol. 10(12), pp. 1775–1777, 1998.

[10] S. Chattopadhyay, P. K. Bose, and C. K. Maiti, "Photoresponse of $Si_{1-x}Ge_x$ heteroepitaxial p-i-n photodiodes," *Solid-State Electron*., vol. 43(9), pp. 1741–1745, 1999.

[11] L. Colace, G. Masini, and G. Assanto, "Ge-on-Si approaches to the detection of near-infrared light," *IEEE J Quantum Electron*., vol. 35(12), pp. 1843–1852, 1999.

[12] R. L. Jiang, Z. Y. Lo, W. M. Chen, L. Zang, S. M. Zhu, X. B. Liu, X. M. Cheng, Z. Z. Chen, P. Chen, P. Han, and Y. D. Zheng, "Normal-incidence SiGe/Si photodectectors with different buffer layers," *J Vac. Sci. Technol. B*, vol. 18(3), pp. 1251–1253, 2000.

[13] C. Li, Q. Q. Yang, H. J. Wang, J. L. Zhu, L. P. Luo, J. Z. Yu, and Q. M. Wang, "$Si_{1-x}Ge_x$/Si resonant-cavity-enhanced photodetectors with a solicon-on-oxide reflector operating near 1.3 μm," *Appl. Phys. Lett.*, vol. 77(2), pp. 157–159, 2000.

[14] Zhiyun Lo, Ruolian Jiang, Youdou Zheng, Lan Zang, Zhizhong Chen, Shunming Zhu, Xuemei Cheng, and Xiabing Liu, "Staircase band gap $Si_{1-x}Ge_x$/Si photodetectors," *Appl. Phys. Lett.*, vol. 77(10), pp. 1548–1550, 2000.

[15] D. Krapf, B. Adoram, J. Shappir, A. Saar, S. G. Thomas, J. L. Liu, and K. L. Wang, "Infrared multispectral detection using Si/Si_xGe_{1-x} quantum well infrared photodetectors," *Appl. Phys. Lett.*, vol. 78(4), pp. 495–497, 2001.

[16] R. A. Soref, "Silicn-based group IV heterostructures for optoelectronic applications," *J. Vac. Sci. Technol. A*, vol. 14(3), pp. 913–918, 1996.

[17] R. A. Soref, Z. Atzman, F. Shaapur, M. Robinson, and R. Westhoff, "Infrared waveguide in $Si_{1-x-y}Ge_xC_y$ upon silicon," *Opt. Lett*., vol. 21(5), pp. 345–347, 1996.

[18] F. Y. Huang, K. Sakamoto, K. L. Wang, P. Trinh, and B. Jalali, "Epitaxial SiGeC waveguide photodetector grown on Si substrate with response in the 1.3–1.55-μm wavelength range," *IEEE Photon. Technol. Lett*., vol. 9(2), pp. 229–231, 1997.

[19] F. Y. Huang, K. L. Wang, "Normal-incidence epitaxial SiGeC photodetector near 1.3 μm wavelength grown on Si substrate," *Appl. Phys. Lett*., vol. 69(16), pp. 2330–2332, 1996.

[20] S. S. Iyer, K. Eberl, M. S. Goorsky, F. K. LeGoues, J. C. Tsang, and F. Cardone, "Synthesis of $Si_{1-y}C_y$ alloys by molecular beam epitaxy," *Appl. Phys. Lett.*, vol. 20(3), pp. 356–358, 1992.

[21] R. Braunstein, A. R. Moore, and F. Herman, "Intrinsic optical absorption in germanium-silicon alloy," *Phys. Rev*., vol. 109(3), pp. 695–710, 1958.

[22] R. A. Soref, "Optical band gap of the ternary semiconductor $Si_{1-x-y}Ge_xC_y$," *J. Appl. Phys.*, vol. 70(4), pp. 2470–2472, 1991.

[23] K. Eberl, K. Brunner, and O. Schmidt, *$Si_{1-y}C_y$ and $Si_{1-x-y}Ge_xC_y$ alloy layers*, *Semiconductors and semimetals*, vol. 56, Chapter 8, San Diego: Academic Press, 1999, p. 407.

[24] H. J. Osten, E. Bugiel, and P. Zaumseil, "Growth of an inverse tetragonal distorted SiGe layer on Si(001) by adding small amounts of carbon," *Appl. Phys. Lett.*, vol. 64(25), pp. 3440–3442, 1994.

[25] S. C. Jain, H. J. Osten, B. Dietrich, and H. Rucker, "Growth and properties of strained $Si_{1-x-y}Ge_xC_y$ layers," *Semocond. Sci. Technol*., vol. 10, pp. 1289–1302, 1995.

[26] J. L. Regolini, S. Bodhar, J. C. Oberlin, F. Ferrieu, G. Gauneau, B. Lambert, and P. Boucaud, "Strain compensated heterostructures in the $Si_{1-x-y}Ge_xC_y$ ternary system," *J. Vac. Sci. Technol. A*, vol. 12, pp. 1015–1019, 1994.

[27] D. C. Houthton, "Strain relaxation kinetics in $Si_{1-x}Ge_x$/Si heterostructures," *J. Appl. Phys.*, vol. 70(4), pp. 2136–2151, 1991.

Baojun Li received the B.Sc degree in Physics in 1987 from the Northwest Normal University, Lanzhou, China, the M.Sc degree in Semiconductor Physics and Semiconductor Device Physics in 1993 from Lanzhou University, China, and the

Ph.D degree in Electronic Engineering in 1998 from Xi'an Jiaotiong University, China.

From 1998 to 2000, he was with the Surface Physics National Key Laboratory, Fudan University, Shanghai, China, where he was a Postdoctoral Fellow and worked in the area of SiGe-based optoelectronic devices and monolithic integration. Since 2000, he was with the Advanced Materials for Micro- & Nano- Systems, Singapore-MIT Alliance, where he was a Postdoctoral Fellow and was promoted to a Research Fellow in 2001. His current research interests are optoelectronic and photonic devices. He has published over 40 papers and holds one USA patent.

Dr. Li awarded the first-class prize of provincial science and technology progress in 1994, the most outstanding young teacher of Gansu Province in 1994, the most outstanding Ph.D. candidate in Xi'an Jiaotong University in 1996 and 1997, respectively, and one of the top six authors in China selected by China Science Daily for published papers of National Natural Science Foundation of China in 1998, etc.

Soo-Jin Chua graduated with a B.Eng (Hons) from the University of Singapore in 1974 and his PhD from the University of Wales, United Kingdom in 1977. In 1978, he worked for the Standard Telecommunications Labs, Harlow, UK. In 1981, he spent a year at the Fraunhofer Institute of Semiconductor Technology, Munich under a German Exchange Scholarship (DAAD). He was a Visiting Fellow of Japan Society for the Promotion of Science in 1988 and of the British Council in 1990. Currently, he is Professor of Optoelectronics in the Department of Electrical and Computer Engineering, National University of Singapore, Deputy Director of the Singapore-MIT Alliance (SMA) and Director of the Opto and Electronics Cluster, Institute of Materials Research and Engineering (IMRE). His research area is in optoelectronics and has published over 150 papers in international journals.

Dr Chua is Sr. member of IEEE. He served as Chairman of IEEE, Singapore Chapter from 1984 to 1986 and as Chairman of Education Committee, Region 10 from 1987 to 1988.

E. A. Fitzgerald, photograph and biography not available at the time of publication.

C. W. Leitz, photograph and biography not available at the time of publication

Lingyun Miao received the B.Eng. degree in Thermal Engineering in July 1999, from Tsinghua University, China and the M.Eng. degree in Advanced Materials in July 2001, from Singapore-MIT Alliance (SMA). Currently, he is a Research Officer in the Opto and Electronics Cluster, Institute of Materials Research and Engineering (IMRE).